Materials Advances

ROYAL SOCIETY OF CHEMISTRY

PAPER

View Article Online
View Journal | View Issue

Cite this: *Mater. Adv.*, 2025, 6, 3851

Novel bio-chelating agent-assisted eco-friendly synthesis of $Sr_{0.9}X_{0.1}CoO_{3-\delta}$ (X = Ba, Ce) perovskite electrodes for supercapacitor applications

Muneeb Irshad, *[a] Muhammad Asif,[a] Muhammad Salim Butt,[b] Muhammad Rafique, [c] Misbah Durrani[a] and Ahmed M. Fouda[d]

The current work pioneers the synthesis of a novel composition of $Sr_{0.9}X_{0.1}CoO_{3-\delta}$ (X = Ba, Ce) perovskite electrode materials for supercapacitors through an innovative semi-green route, utilizing lemon powder as the bio-chelating agent. The synergy between the biomolecules and organic citric acid in lemon powder resulted in minimal impurities and enhanced the crystallinity of the desired perovskite electrodes. XRD analysis confirmed the cubic perovskite structure of all $Sr_{0.9}X_{0.1}CoO_{3-\delta}$ (X = Ba, Ce) perovskite electrodes synthesized *via* both semi-green and chemical approaches. Notably, samples synthesized through the semi-green approach exhibited better crystallinity with no secondary phases. Microstructural analysis revealed a dense and agglomerated morphology for all samples, while EDX analysis confirmed the elemental composition with no prominent impurities. FTIR analysis confirmed the presence of identical functional groups in samples synthesized through both routes. Electrochemical studies demonstrated the highest specific capacitance of 1176.36 F g^{-1} and excellent electrochemical stability, with 88.2% capacity retention after 5000 galvanostatic charge–discharge cycles for $Sr_{0.9}X_{0.1}CoO_{3-\delta}$ (X = Ce) synthesized through the semi-green route. Meanwhile, $Sr_{0.9}X_{0.1}CoO_{3-\delta}$ (X = Ba) also exhibited a reasonable specific capacitance. These findings confirm that the novel perovskite composition $Sr_{0.9}X_{0.1}CoO_{3-\delta}$ (X = Ba, Ce) can be successfully utilized for supercapacitor applications and that the innovative semi-green route can also be employed for the efficient synthesis of perovskite materials, ensuring minimal ecological impact and reduced impurities compared to conventional chemical and green synthesis routes.

Received 6th December 2024,
Accepted 19th April 2025

DOI: 10.1039/d4ma01199f

rsc.li/materials-advances

1. Introduction

In the modern era, there is a dire need to explore energy devices that are sustainable, environmentally friendly, and capable of providing quick responsiveness with high energy and power densities.[1] Supercapacitors (SCs) have emerged in recent years as a promising energy storage technology due to their high cyclic stability, high power density, and fast charging/discharging rates.[2–4] Many applications require high power rather than high energy, such as phone chargers, regenerative braking systems, and portable vacuum cleaners.[5,6] Therefore, supercapacitors can serve as an alternative to conventional lithium-ion batteries.[7] Supercapacitors are intermediate between conventional capacitors and rechargeable batteries, but they have a similar configuration with two electrodes—an anode and cathode—immersed in an electrolyte, separated by a membrane.[8]

There are two types of supercapacitors based on the charge storage mechanism: electrical double-layer capacitors (EDLCs) and pseudocapacitors.[9,10] In EDLCs, charge is stored electrostatically at the interface between the electrolyte and the surface of the electrodes without any faradaic reaction (referred to as non-faradaic). During charging, the ions in the electrolyte move toward their respective electrodes, and an inner Helmholtz layer is formed, known as the double layer, which enhances the specific capacitance.[11–13] In pseudocapacitors, the charge storage mechanism is achieved through redox reactions (oxidation–reduction), electrosorption, or ion intercalation mechanisms.[14] Thus, pseudocapacitors store charge both electrostatically and electrochemically, leading to higher specific capacitance than EDLCs. Carbon-based materials are commonly used as electrode materials in EDLCs due to their facile processing, chemical

[a] *Department of Physics, University of Engineering and Technology, Lahore 54890, Pakistan. E-mail: muneebirshad@gmail.com, muneeb_irshad@uet.edu.pk*
[b] *Department of Electrical Engineering, University of Engineering and Technology, New Campus, Lahore 39021, Pakistan*
[c] *Department of Physics, University of Sahiwal, Sahiwal 57000, Pakistan*
[d] *Department of Chemistry, Faculty of Science, King Khalid University, Abha, Saudi Arabia*

stability, wide operational temperature range, ability to function without binder agents, and well-established activation techniques.[15] EDLCs store the charge at their electrochemical surfaces; however, they have some drawback, such as a low energy density and specific capacitance, along with excessive cost.[13,16] Pseudocapacitive-type materials, on the other hand, exhibit higher energy densities but possess shorter life cycles. The shorter life cycles of pseudocapacitive materials can be improved by employing conductive, sustainable methods to synthesize transition metal oxides.[17] Chi-Chang Hu *et al.* first reported that RuO, a transition metal oxide, showed pseudocapacitive behavior due to its various corrosive states that made the faradaic process possible. However, while much work followed on transition metal oxides in this field, they are generally too costly.[18,19] Meanwhile, perovskite oxides have attracted increasing attraction for different applications and now as potential electrode materials in supercapacitors due to their structural flexibility, low cost, high charge-carrier mobility, compositional and stoichiometric flexibility, high tapping density, and appropriate oxygen vacancies.[9,20] The presence of oxygen vacancies in perovskite-based materials makes the intercalation process faster than in transition metal oxides. Various perovskite oxides have been investigated as active materials for SCs due to their high number of oxygen vacancies and high tapping density.[21] Recently, SrCoO has been explored as a potential electrode material for supercapacitors. It has been reported that $SrCoO_{3-\delta}$ perovskite with a cubic structure exhibits higher conductivity than other structures, but it faces issues with achieving structural stability at room temperature.[22] However, it has been reported that doping different dopants at the A or B site can help $SrCoO_{3-\delta}$ attain structural stability. Furthermore, it was found that the substitution of a mere 5% can introduce significant changes in the conductivity, structure, and oxygen diffusion of perovskite structures. It has also been reported that dopants such as Ce^{4+}, Y^{4+}, Zr^{4+}, Al^{3+}, and Sc^{3+} can increase the oxygen permeability and conductivity of perovskites by 1–2 orders of magnitude due to the high concentrations of oxygen vacancies present.[23–26] Considering the aforementioned findings, the doping of SrCoO with Ba and Ce could be expected to have a significant impact on the structural stability and conductivity of $SrCoO_{3-\delta}$. It was previously reported that the larger ionic radii of Ba ions than Sr ions would cause lattice distortions and lead to the formation of more oxygen vacancies to maintain charge neutrality.[27] Similarly, Ce doping can also lead to the formation of oxygen vacancies. This is because Ce can exist in multiple oxidation states, primarily Ce^{3+} and Ce^{4+}, and the transition between these states can lead to the formation or annihilation of oxygen vacancies to maintain charge neutrality.[28] Generally, the charge-storage capacity of the perovskites is dependent on the availability of oxygen vacancies, and therefore, the doping of Ba and Ce in $SrCoO_{3-\delta}$ would not only lead to enhanced electrochemical performance for supercapacitor electrodes but at the same time would also improve their structural stability.[29,30]

In addition to the investigation of the novel composition of $Sr_{0.9}X_{0.1}CoO_{3-\delta}$ (X = Ba, Ce) as perovskite electrodes for supercapacitors, the current project also developed an innovative synthesis approach in which organic citric acid (lemon) and biomolecules played a synergistic role as reducing and capping agents to facilitate the synthesis of $Sr_{0.9}X_{0.1}CoO_{3-\delta}$ (X = Ba, Ce) for the first time. Although chemical approaches are commonly used to synthesize perovskites, they involve the use of hazardous solvents and reagents, posing substantial ecological and health concerns.[31] In contrast, the reported green approach can mitigate these concerns, but the end product obtained through green approach lacks phase purity and the desired crystallinity, and suffers from a reduced reproducibility, and lower yield.[32] Therefore, balancing the efficiency and environmental impact of both synthesis routes remains a critical challenge for the advancement of perovskite technology. The novel approach we propose can attain this balance by simultaneously utilizing the reducing and capping role of both biomolecules and organic citric acid present in lemon to synthesize $Sr_{0.9}X_{0.1}CoO_{3-\delta}$ (X = Ba, Ce) perovskite electrodes.

Herein, the $Sr_{0.9}X_{0.1}CoO_{3-\delta}$ (X = Ba, Ce) perovskite composition was synthesized for the first time for use as electrodes for pseudocapacitive applications. In addition, an innovative semi-green approach was also employed to synthesize this novel composition along with a conventional chemical approach for comparison. Our novel semi-green approach utilized the synergy of biomolecules and the organic citric acid present in lemon as reducing and capping agents, which enabled more control over the synthesis process, together with minimized toxicity compared to the conventional approach and impurities compared to the green approach. The synthesized electrodes were investigated through various characterizations.

2. Experimental section

Semi-green and chemical combustion methods were employed to synthesize $Sr_{0.9}X_{0.1}CoO_{3-\delta}$ (X = Ba, Ce) as anode materials for supercapacitors. The starting precursors Sr $(NO_3)_2$, Co $(NO_3)_2{\cdot}6H_2O$, Ba $(NO_3)_2{\cdot}6H_2O$, and Ce $(NO_3)_2{\cdot}6H_2O$ in an exact stoichiometric ratio were dissolved in 200 mL deionized water under constant stirring and heating to prepare a transparent solution. Lemon powder (LP) and citric acid (CA) were used as chelating agents in 20–21 wt% of the total precursor solution. Next, the clear precursor solution was put in a ceramic beaker, and placed on a magnetic hot plate. The solution was continuously stirred and heated at 80 °C on the hot plate. The viscosity of the homogeneous solution was increased by boiling off the water and it changed into a gel at 110 °C. Further heating evaporated all the water from the pores of the gel and this then self-ignited to produce a fine powder of perovskite materials. The obtained powder was then calcinated at 200 °C for 1 h and then sintered at 1150 °C for 5 h to obtain a further fine powder. The complete synthesis process is illustrated schematically in Fig. 1. Pellets of the sintered powder were formed using a hydraulic press under a pressure of 300 MPa and the samples were then characterized by different techniques, including XRD, FESEM, EDX, FTIR, CV and GCD.

All the synthesized samples were characterized by X-ray diffraction (XRD), scanning electron microscopy (SEM), energy dispersive X-ray spectroscopy (EDX) and Fourier-transform

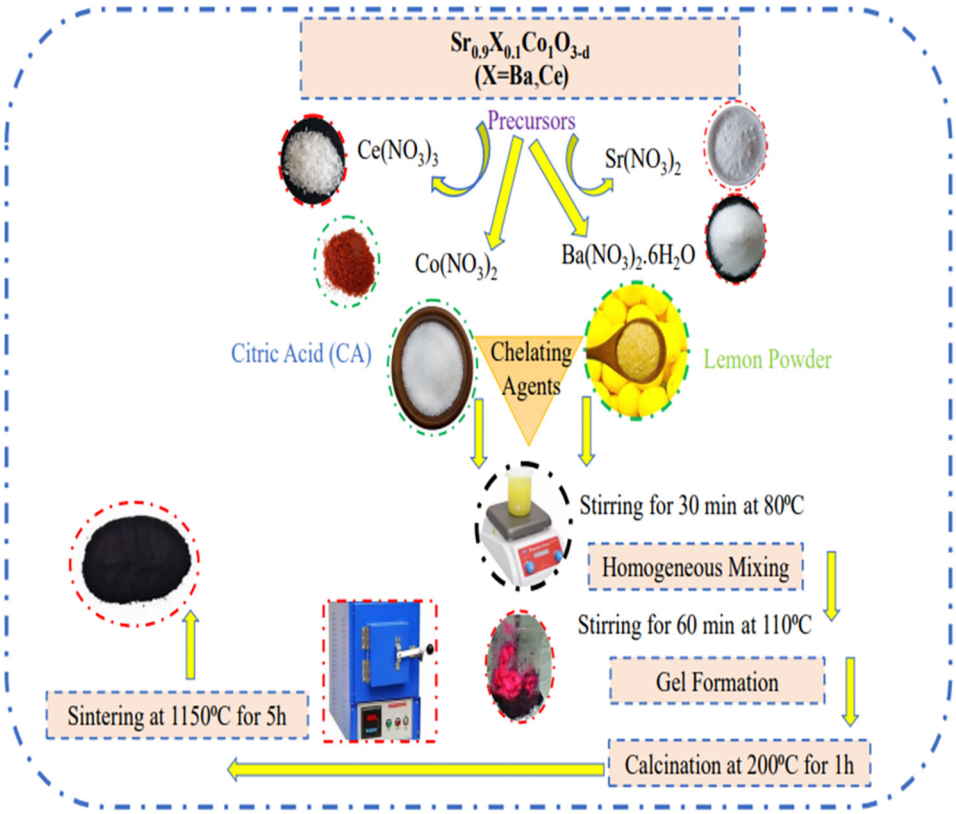

Fig. 1 Schematic of $Sr_{0.9}X_{0.1}CoO_{3-\delta}$ (X = Ba, Ce) perovskite anode materials synthesized through semi-green (LP) and chemical (CA) approaches.

infrared spectroscopy (FTIR) to study their structural properties, morphology, elemental composition, and functional groups. The electrochemical performances of the synthesized electrodes in a 1 M KOH electrolyte solution were assessed by cyclic voltammetry (CV) and galvanostatic charge–discharge (GCD) analyses.

3. Results and discussions

Fig. 2 represents the XRD spectra of $Sr_{0.9}X_{0.1}CoO_{3-\delta}$ (X = Ba, Ce) synthesized through semi-green (LP) and chemical (CA) approaches. The diffraction planes (100), (101), (110), (111), (200), (211), (220) and (221) confirmed their cubic structure (JCPDS = 00-038-1148) with the space group *Pm3m* for all the $Sr_{0.9}X_{0.1}CoO_{3-\delta}$ (X = Ba, Ce) samples synthesized with either the semi-green (LP) or chemical (CA) approach.

It was clear that $Sr_{0.9}X_{0.1}CoO_{3-\delta}$ synthesized by the semi-green (LP) synthesis exhibited no secondary phases. Meanwhile, it was interesting to observe that $Sr_{0.9}X_{0.1}CoO_{3-\delta}$ (X = Ba) synthesized with the chemical approach exhibited a secondary phase of BaO, which was unexpected for the chemical approach. The presence of this secondary phase could be attributed to the low sintering temperature, as previously reported by researchers, wherein the BaO phase appeared for samples sintered at temperatures lower than 1400 °C.[33–38] The absence of BaO in $Sr_{0.9}X_{0.1}CoO_{3-\delta}$ (X = Ba) synthesized with the semi-green (LP) approach could be credited to the presence of metallic impurities, which may have acted as a sintering aid.

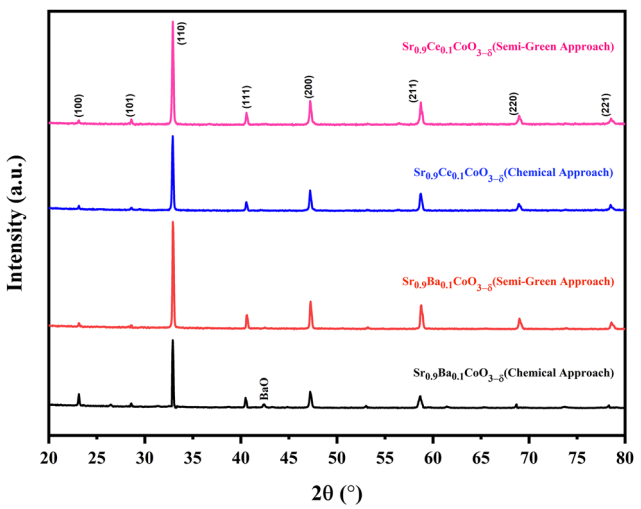

Fig. 2 XRD spectra of $Sr_{0.9}X_{0.1}CoO_{3-\delta}$ (X = Ba, Ce) synthesized through semi-green and chemical approaches, showing the cubic perovskite structure for all samples with no extra phases. However, a small BaO phase appeared for $Sr_{0.9}Ba_{0.1}O_{3-\delta}$ synthesized through the chemical approach.

Table 1 presents the variations in the structural parameters, such as crystallite size, dislocation density, microstrain, and lattice constant, for $Sr_{0.9}X_{0.1}Co\ O_{3-\delta}$ synthesized through the semi-green (LP) and chemical (CA) approaches.

Table 1 Structural parameters of $Sr_{0.9}X_{0.1}CoO_{3-\delta}$ perovskite anodes, showing larger crystallite size for the semi-green (LP)-synthesized anodes compared to the chemically (CA)-synthesized anodes

Sample	Crystallite size (nm)	Lattice constant (nm)	Dislocation density (m^{-2})	Microstrain (nm)
$Sr_{0.9}Ce_{0.1}CoO$ (semi-green method)	49	0.072731	0.401214	0.002452
$Sr_{0.9}Ce_{0.1}CoO$ (chemical method)	47	0.072745	0.446863	0.002586
$Sr_{0.9}Ba_{0.1}CoO$ (semi-green method)	56	0.072764	0.317514	0.00218
$Sr_{0.9}Ba_{0.1}CoO$ (chemical method)	52	0.072804	0.367166	0.002343

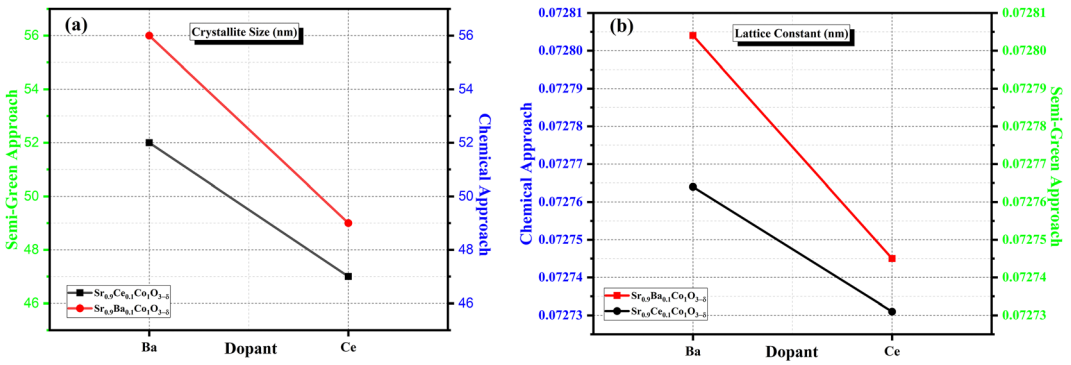

Fig. 3 Variation of (a) crystallite size and (b) lattice constant for the (110) plane of $Sr_{0.9}X_{0.1}CoO_{3-\delta}$ (X = Ba, Ce) synthesized through semi-green (LP) and chemical (CA) approaches.

Fig. 3(a) and (b) present the crystallite sizes and lattice constants of $Sr_{0.9}X_{0.1}Co\ O_{3-\delta}$ (X = Ba, Ce) perovskite anodes synthesized through the semi-green (LP) and chemical (CA) routes. It is clear from Fig. 3(a) that the crystallite sizes of $Sr_{0.9}X_{0.1}Co\ O_{3-\delta}$ (X = Ba, Ce) synthesized by the semi-green (LP) approach were larger than those obtained from the chemical (CA) approach, which could be ascribed to the fact that LP contained metallic impurities, such as Mg and Ca, which may act as a sintering aid to promote crystal diffusion, and hence the crystallite size increased.[39–41]

It can be further inferred from Table 1 and Fig. 3(a) that comparing the semi-green (LP) and chemically (CA) synthesized $Sr_{0.9}X_{0.1}CoO_{3-\delta}$ and $Sr_{0.9}Ba_{0.1}CoO_{3-\delta}$, $Sr_{0.9}Ba_{0.1}CoO_{3-\delta}$ exhibited a larger crystallite size than $Sr_{0.9}Ce_{0.1}CoO_{3-\delta}$, which implies that Ba ions have larger ionic radii and with their incorporation in the lattice they occupy the interstitial sites, leading to lattice expansion and larger grain boundaries.[42] Another reason for the small crystallite of $Sr_{0.9}Ce_{0.1}CoO_{3-\delta}$ compared to $Sr_{0.9}Ba_{0.1}CoO_{3-\delta}$ is the small ionic radii of Ce ions, resulting in the effective incorporation of Ce into the lattice, which may enhance the grain boundary formation and inhibit the grain growth, leading to finer crystallites.[43]

Similarly, Fig. 3(b) presents the variation of the lattice constant of $Sr_{0.9}X_{0.1}CoO_{3-\delta}$ (X = Ba, Ce) synthesized through the semi-green (LP) and chemical (CA) approaches, showing the smaller lattice constant for the semi-green synthesis, which may be ascribed to the fact that the sustainable approach (LP) improved the crystallinity leading to smaller defect densities in the lattice formation.[44] It can be further inferred from Table 1 and Fig. 3(b) that $Sr_{0.9}Ce_{0.1}CoO_{3-\delta}$ had a smaller lattice constant compared to $Sr_{0.9}Ba_{0.1}CoO_{3-\delta}$, which was ascribed to the small difference in the ionic radii of Ce ions compared to Ba ions.[45]

Fig. 4(a) and (b) present the variation of the dislocation density and microstrain of $Sr_{0.9}X_{0.1}CoO_{3-\delta}$ (X = Ba, Ce)

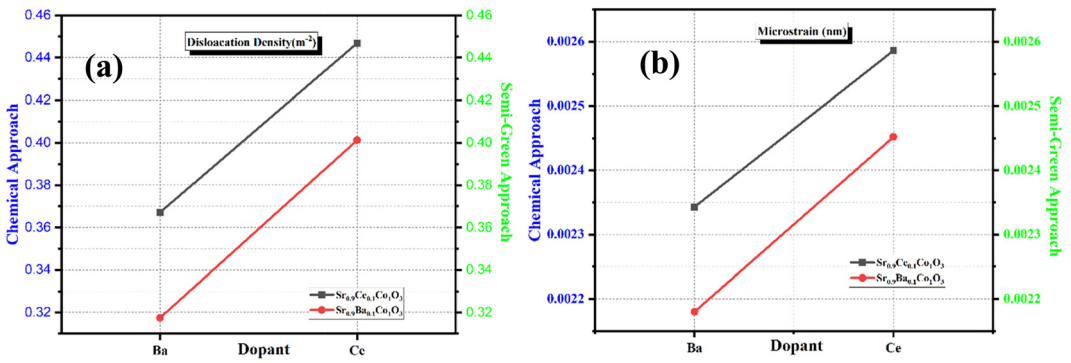

Fig. 4 Variation of (a) dislocation density and (b) microstrain for the (110) plane of $Sr_{0.9}X_{0.1}CoO_{3-\delta}$ (X = Ba, Ce) synthesized through the semi-green (LP) and chemical (CA) approaches.

synthesized through the two approaches (semi-green and chemical). It is clear from Fig. 4(a) that the dislocation density was higher for the semi-green (LP) method due to the presence of metallic impurities, which influenced the lattice symmetry and led to larger dislocations.[46] It can be observed from Fig. 4(b) that the samples synthesized by the semi-green (LP) route had larger microstrain compared to those synthesized by the chemical (CA) route due to the presence of metallic impurities, such as Mg and Ca; whereby the semi-green method led to higher lattice distortions. Similarly, $Sr_{0.9}Ce_{0.1}CoO_{3-\delta}$ showed higher microstrain than $Sr_{0.9}Ba_{0.1}CoO_{3-\delta}$, which may be due to the higher valency of Ce^{3+} than Ba^{2+}, thus more oxygen vacancies were produced and resulting in higher lattice distortion in the unit cell,[42,47] as shown in Fig. 4(b).

4. Scanning electron microscopy (SEM) analysis

Fig. 5(a)–(d) present the SEM images of $Sr_{0.9}X_{0.1}CoO_{3-\delta}$ synthesized through the semi-green (LP) and chemical (CA) routes, while Fig. 5(e)–(h) show their corresponding histograms. It is clear from the SEM image (Fig. 5(a)) of the $Sr_{0.9}Ba_{0.1}CoO_{3-\delta}$ anode synthesized through the semi-green (LP) approach that it exhibited a regular and porous structure with a more defined shape and less agglomeration compared to the $Sr_{0.9}Ba_{0.1}CoO_{3-\delta}$ anode (Fig. 5(b)) synthesized with the chemical (CA) approach, which could be credited to the presence of biomolecules and organic citric acid present in the lemon powder. It has been reported that biomolecules present in organic compounds can act as both reducing and capping agents during the semi-green synthesis; therefore, the combined effect of organic citric acid and biomolecules present in the lemon powder can provide more control over the growth and agglomeration of the nanoparticles.[48–50] The microstructure of the $Sr_{0.9}Ba_{0.1}CoO_{3-\delta}$ anode synthesized through the chemical method showed irregular particle shapes with multiple crevices and protrusions, indicating the heterogeneous nature of the particles. Fig. 5(e) and (f) show the range of the $Sr_{0.9}Ba_{0.1}CoO_{3-\delta}$ anodes' particle sizes synthesized by the two approaches. It is evident from the statistical histogram (Fig. 5(e)) that the particle size of $Sr_{0.9}Ba_{0.1}CoO_{3-\delta}$ synthesized through the semi-green (LP) route ranged from 10–55 nm, with most particles existing in the 20–25 nm range, while the particles for the $Sr_{0.9}Ba_{0.1}CoO_{3-\delta}$ anode synthesized through the chemical (CA) route lay in a wider range from 10–110 nm, with most particles existing in the 80–90 nm range. This variation in the particle sizes of the $Sr_{0.9}Ba_{0.1}CoO_{3-\delta}$ synthesized through the two routes clearly showed that the synergistic role of natural citric acid and biomolecules in the semi-green (LP) route effectively reduced and capped the $Sr_{0.9}Ba_{0.1}CoO_{3-\delta}$ compared to the chemical synthesis route, where only synthetic citric acid acted as the reducing and capping agent.[51,52]

The microstructures of $Sr_{0.9}Ce_{0.1}CoO_{3-\delta}$ synthesized through both approaches are shown in Fig. 5(c) and (d), while the corresponding histograms for the particle sizes are shown in Fig. 5(g) and (h). The $Sr_{0.9}Ce_{0.1}CoO_{3-\delta}$ anode exhibited a similar pattern to that of $Sr_{0.9}Ba_{0.1}CoO_{3-\delta}$, whereby the $Sr_{0.9}Ce_{0.1}CoO_{3-\delta}$ anode particles synthesized through the semi-green (LP) route exhibited small and round particles with less agglomeration, while the chemically synthesized $Sr_{0.9}Ce_{0.1}CoO_{3-\delta}$ anode had larger and more agglomerated particles. The particle sizes of the semi-green-synthesized $Sr_{0.9}Ce_{0.1}CoO_{3-\delta}$ lay in the 4–24 nm range, with most particles existing in the 8–12 nm range, whereas the sizes of the chemically synthesized particles were in the 10–120 nm range, with most particles having a size of 40–50 nm.

It can be further inferred from Fig. 5(a) and (d) that between the semi-green (LP) and chemically (CA) synthesized $Sr_{0.9}Ce_{0.1}CoO_{3-\delta}$ and $Sr_{0.9}Ba_{0.1}CoO_{3-\delta}$, $Sr_{0.9}Ba_{0.1}CoO_{3-\delta}$ exhibited larger crystallite sizes compared to $Sr_{0.9}Ce_{0.1}CoO_{3-\delta}$, which implies that the Ce ions in $Sr_{0.9}Ce_{0.1}CoO_{3-\delta}$ can act as nucleation sites, facilitating the production of nuclei during the synthesis process. Ce can accelerate crystal growth by occupying these favorable sites, providing stable anchoring points for the precursor molecules to attach and arrange themselves, thus facilitating nucleation, resulting in the formation of smaller particles with a more uniform size distribution.

5. EDX analysis

Fig. 6(a)–(d) present the EDX spectra of the $Sr_{0.9}X_{0.1}CoO_{3-\delta}$ anode materials synthesized through the semi-green (LP) and chemical (CA) routes. The surface areas were carefully selected for the EDX analysis to avoid surface contaminants. The qualitative spectra shown in Fig. 6(a)–(d) confirmed the presence of strontium, cobalt, and oxygen in all the samples, while Ba and Ce were confirmed in $Sr_{0.9}Ba_{0.1}CoO_{3-\delta}$ and $Sr_{0.9}Ce_{0.1}CoO_{3-\delta}$ synthesized by both routes, respectively. The quantitative data shown in the inset provide the percentage elemental compositions of the $Sr_{0.9}X_{0.1}CoO_{3-\delta}$ anode materials. It can be observed from the spectra that no impurity-related peaks appeared, depicting the high purity of the $Sr_{0.9}X_{0.1}CoO_{3-\delta}$ anodes. The absence of impurity-related peaks was unexpected for $Sr_{0.9}X_{0.1}CoO_{3-\delta}$ synthesized through the semi-green (LP) approach because lemon powder contains several minerals, but their absence from the spectra can be ascribed to their concentration being lower than the detection limit of EDX.[53,54] The compositional analysis confirmed that the semi-green route can be employed for the successful synthesis of $Sr_{0.9}X_{0.1}CoO_{3-\delta}$ anodes without significant impurities.

6. Fourier-transform infrared (FTIR) analysis

Fig. 7 depicts the FTIR spectra of $Sr_{0.9}X_{0.1}CoO_{3-\delta}$ (a) doped with Ba, and (b) doped with Ce, synthesized using citric acid and lemon powder as chelating agents. The small peaks around 3735, 2980, 2361, 1461, and 994–911 cm^{-1} were related to O–H stretching, C–H stretching, O═C═O stretching, C–H bending and M–O stretching, respectively, in all the samples. Oxygen vacancies in perovskite oxides may cause hydroxyl groups (OH^-) to develop on the surface. These hydroxyl groups may have originated from the interaction of

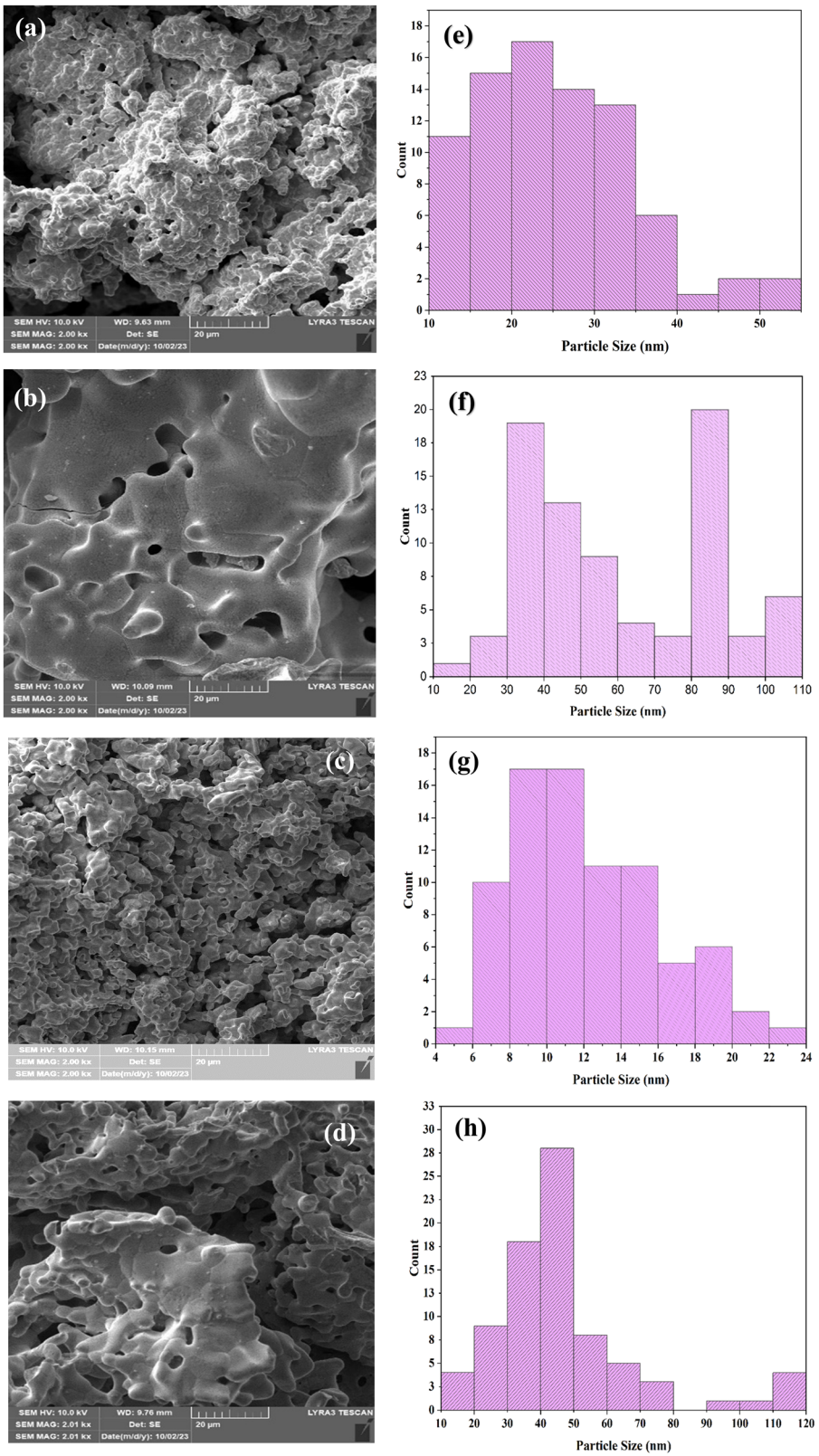

Fig. 5 SEM images and corresponding histograms (a, e) $Sr_{0.9}Ba_{0.1}CoO_{3-\delta}$ anode synthesized through the semi-green (LP) approach, exhibiting a regular and porous structure; and (b, f) $Sr_{0.9}Ba_{0.1}CoO_{3-\delta}$ anode synthesized through the chemical (CA) approach, showing agglomeration; (c, g) $Sr_{0.9}Ce_{0.1}CoO_{3-\delta}$ anode synthesized through the semi-green (LP) approach; and (d, h) $Sr_{0.9}Ce_{0.1}CoO_{3-\delta}$ anode synthesized through the chemical (CA) approach, showing agglomeration.

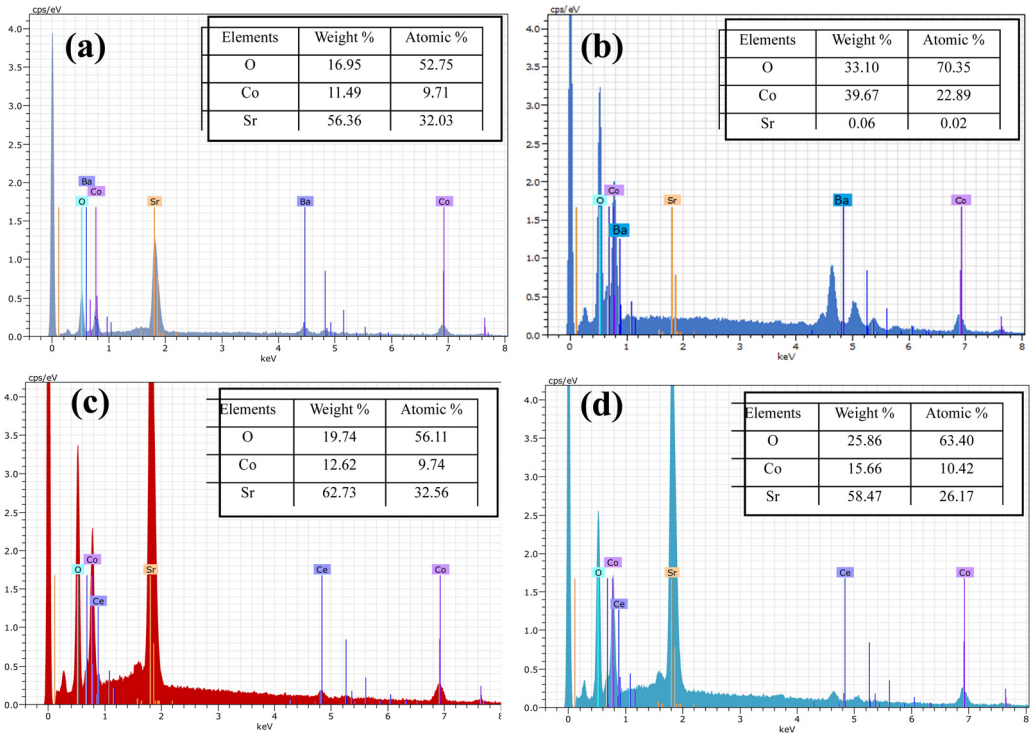

Fig. 6 EDX spectra of $Sr_{0.9}X_{0.1}CoO_{3-\delta}$ (a) doped with (X = Ba) using citric acid as a chelating agent, (b) doped with (X = Ba) using lemon powder as a chelating agent, (c) doped with (X = Ce) using citric acid as a chelating agent, and (d) doped with (X = Ce) using lemon powder as a chelating agent.

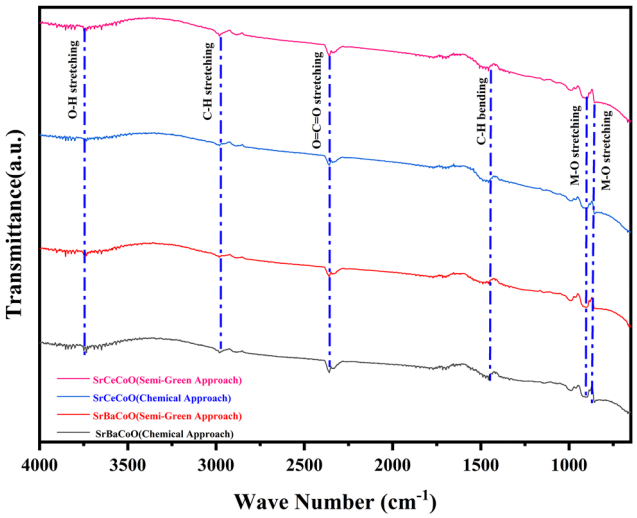

Fig. 7 FTIR spectra of $Sr_{0.9}X_{0.1}CoO_{3-\delta}$ (X = Ba, Ce), synthesized through semi-green (LP) and chemical (CA) approaches.

surface oxygen species with ambient moisture, and may be responsible for the peaks for O–H stretching vibrations in the FTIR spectra.[55] The C–H stretching and bending vibrations may arise due to the presence of organic residue within the synthesized material derived from the chelating agents used, *i.e.*, citric acid and lemon powder. The peaks associated with O═C═O stretching vibrations imply the presence of carbonate species in the produced materials. The existence of carbonate species could be due to ambient CO_2 absorption or residual carbonate from the precursor materials. Also, there was an indication of M–O stretching, which implied the formation of metal oxides, showing the perovskite nature of the samples, as previously reported in the literature.[56–62]

7. Electrochemical analysis

a. Cyclic voltammetry (CV)

The electrochemical performances of the $Sr_{0.9}X_{0.1}CoO_{3-\delta}$ (X = Ba, Ce) perovskite electrodes synthesized through the semi-green (LP) and chemical (CA) approaches were evaluated through cyclic voltammetry and are shown in Fig. 8. Fig. 8(a) displays the CV curves of the $Sr_{0.9}X_{0.1}CoO_{3-\delta}$ (X = Ba, Ce) perovskite electrodes synthesized through the semi-green (LP) and chemical (CA) approaches in 1 M KOH in a potential window range of 0.1–0.8 V at a scan rate of 20 mV s^{-1}. It can be observed from CV curves that all the materials exhibited a pseudocapacitive behavior because of the faradaic redox reactions. Also, these curves displayed rectangular and steep slopes, suggestive of higher power densities.[63] It is clear from Fig. 8(a) that the $Sr_{0.9}X_{0.1}CoO_{3-\delta}$ electrodes synthesized through the semi-green (LP) route exhibited better capacitance compared to the same electrodes synthesized through the chemical (CA) route. The specific capacitance (C_s) of the working electrodes was calculated using the following equation:[64]

$$C_s = \frac{\int I dt}{2 \times M \times S \times \Delta V} \quad (1)$$

The specific capacitances of $Sr_{0.9}Ce_{0.1}CoO_{3-\delta}$ synthesized by the semi-green (LP) and chemical (CA) approaches were 1176

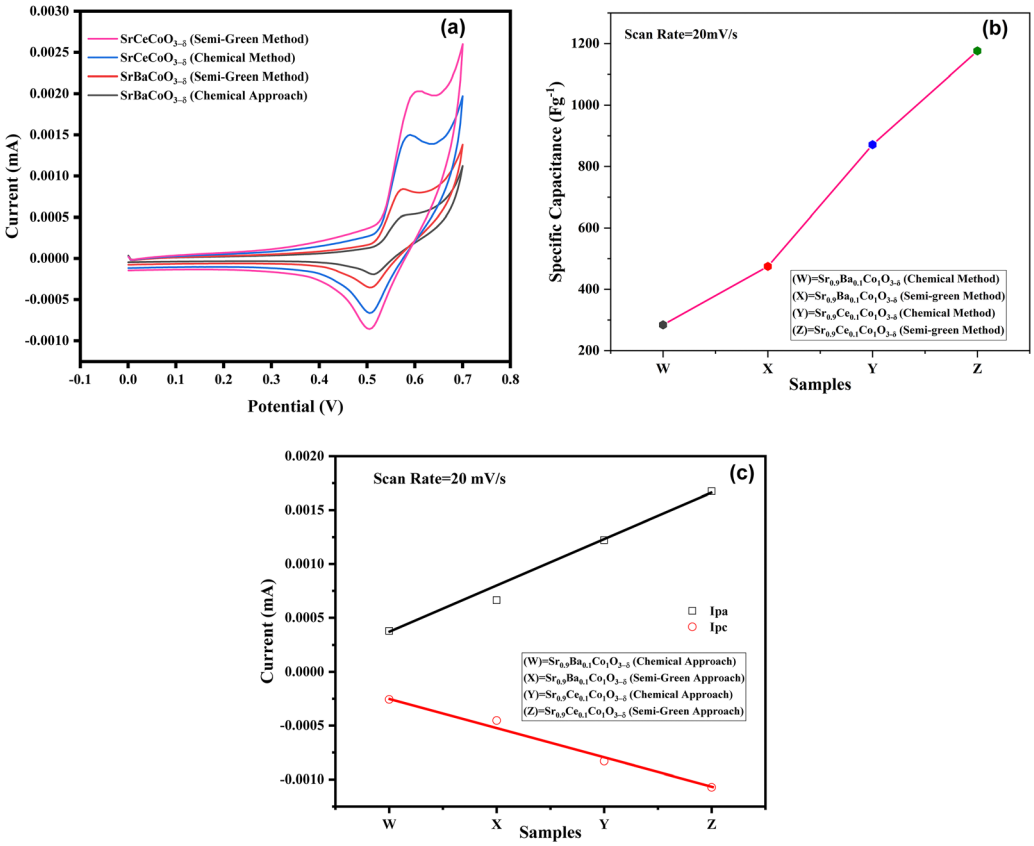

Fig. 8 (a) Cyclic voltammetry curves of $Sr_{0.9}X_{0.1}CoO_{3-\delta}$ (X = Ba, Ce) within the potential window range of −0.1 to 0.7 V at a scan rate of 20 mV s^{-1}. (b) Specific capacitance of $Sr_{0.9}X_{0.1}CoO_{3-\delta}$ (X = Ba, Ce). (c) Anodic and cathodic peak currents obtained from the CV curves of $Sr_{0.9}X_{0.1}CoO_{3-\delta}$ (X = Ba, Ce) synthesized through the semi-green (LP) and chemical (CA) approaches.

and 871 F g^{-1}, respectively, while $Sr_{0.9}Ba_{0.1}CoO_{3-\delta}$ synthesized through the semi-green (LP) and chemical (CA) routes exhibited specific capacitances of 475 and 284 F g^{-1}, respectively, and are depicted in Fig. 8(b). Fig. 8(c) shows the anodic and cathodic current peaks of $Sr_{0.9}X_{0.1}CoO_{3-\delta}$ (X = Ba, Ce) synthesized through both routes. It can be observed from Fig. 8(a)–(c) that the semi-green-synthesized $Sr_{0.9}X_{0.1}CoO_{3-\delta}$ (X = Ba, Ce) electrodes exhibited better capacitance compared to the corresponding chemically synthesized $Sr_{0.9}X_{0.1}CoO_{3-\delta}$ (X = Ba, Ce) electrodes, which could be ascribed to the presence of metallic impurities in the lemon powder, which can facilitate the redox process due to the availability of higher charge carriers. In addition, the large crystallite size of the semi-green-synthesized electrodes compared to the chemically synthesized electrodes may also contribute to the better electrochemical performance.[65] Generally, a larger crystallite size leads to the reduction in the grain boundary resistance, which reduces the number of scattering sites. This permits the electrons to move freely through the material, enhancing the electrical conductivity, which facilitates the charge carriers moving faster, leading to rapid charging and discharging.[66–68]

It was interesting to observe that among the semi-green and chemically synthesized $Sr_{0.9}X_{0.1}CoO_{3-\delta}$ (X = Ba, Ce) electrodes, the $Sr_{0.9}Ce_{0.1}CoO_{3-\delta}$ electrode exhibited better performance compared to $Sr_{0.9}Ba_{0.1}CoO_{3-\delta}$, which could be ascribed to the higher valence state of Ce^{3+} than Ba^{2+}, which can provide more charges, leading to higher oxygen vacancies and resulting in a better electrochemical performance.[69–71]

b. Galvanostatic charge–discharge (GCD)

GCD tests were performed on $Sr_{0.9}X_{0.1}CoO_{3-\delta}$ (X = Ba, Ce) perovskite electrodes synthesized through the semi-green (LP)

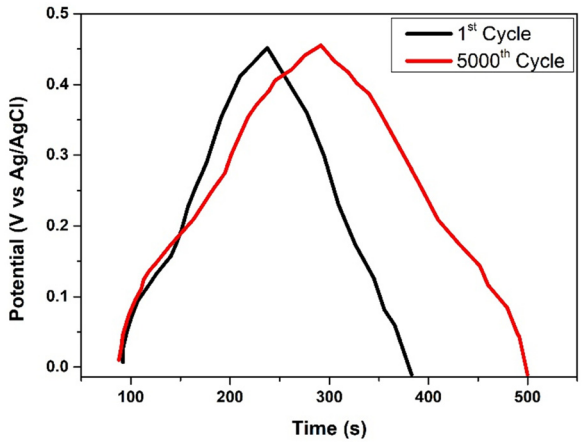

Fig. 9 Galvanostatic charge–discharge (GCD) plots of $Sr_{0.9}X_{0.1}CoO_{3-\delta}$ (X = Ce) perovskite electrodes synthesized through the semi-green (LP) approach, comparing the electrochemical behavior between the 1st and 5000th cycles.

Table 2 Comprehensive comparison of different electrodes

Electrode material	Cycling stability (%)	Charge–discharge rate (A g^{-1})	Operating voltage window (V)	Specific capacitance (F g^{-1})	Ref.
Ni_3Se_4/Co_3Se_4	83.4	1	1.5–1.8	1120.4	75
Reduced graphene oxide	97.14 (5000 cycles)	0.2	0.2–1.0	585.44	76
SbTe/SnSe	96.08 (5000 cycles)	1–3	0.1–0.7	1276	77
$RGO/LaAlO_3$	55.47 (5000 cycles)	0.5	0–1.2	283	78
$La_{0.75}Sr_{0.25}Cr_{0.5}Mn_{0.5}O_3$ LSCM	92 (5000 cycles)	10	0.2–1.0	630	79

Table 3 Performance metrics of some reported green-synthesized perovskite-based supercapacitors

Electrode material	Synthesis approach	Energy density (W h kg^{-1})	Power density (W kg^{-1})	Specific capacitance (F g^{-1})	Ref.
$LaMnO_3$	Green synthesis (Lemon juice)	52.5	1000	375	80
$RGO/LaAlO_3$	Green synthesis (Green tea)	57	569	721	78
Ag-Zirconia	Green synthesis (*Sauropus androgynus*)	31.94	500.86	256	81
$KMnCl_3/C_{60}$	Antisolvent (KCl and $MnCl_2$)	150.58	3.1	936	82
$SnO_2/g\text{-}C_3N_4$	Green synthesis (*Ananas comosus*)	11.5	1705	302.7	83

and chemical (CA) approaches. These tests, conducted in 1 M KOH electrolyte within a 0–0.45 V potential window (*vs.* Ag/AgCl), compared the electrochemical behavior between the 1st and 5000th cycles. Fig. 9 depicts the GCD curves of $Sr_{0.9}Ce_{0.1}CoO_{3-\delta}$ for both the 1st and 5000th cycles, highlighting the material's impressive performance over extended cycling. Notably, the GCD tests revealed exceptional capacity retention after 5000 cycles, as evidenced by the comparative curves in Fig. 9, showing that the semi-green-synthesized $Sr_{0.9}Ce_{0.1}CoO_{3-\delta}$ yielded a specific capacitance of 1176 F g^{-1} with 88.2% capacitance retention after 5000 cycles, demonstrating performance comparable to, and in some instances surpassing, previously reported perovskite materials. For example, MnO_2@$SrCo_{0.875}Nb_{0.125}O_3$@CC exhibited a specific capacitance of 2066.0 mF cm^{-2},[72] while $SrFe_{0.85}Zr_{0.15}O_{3-\delta}$ achieved a specific capacitance of 163.92 F g^{-1}.[73] Similarly, Ti-substituted $SrCo_{0.9}Ti_{0.1}O_{3-\delta}$ delivered a specific capacitance of 625.0 F g^{-1}, attributed to its stable cubic structure and abundant oxygen vacancies.[22] Cr-substituted $SrCo_{0.95}Cr_{0.05}O_{3-\delta}$@CC, reported by Jiahao *et al.*, maintained 95.8% capacitance after 10 000 cycles in an asymmetric configuration with PPy@CC.[74] Other perovskites, such as $SrCoO_{2.5}$ (475 F g^{-1}, 85% retention after 2000 cycles) and $LaMnO_3$-based electrodes (720 F g^{-1}, 80% retention after 3000 cycles), have also been documented.[27,29] Table 2 provides a further comprehensive comparison among different supercapacitor electrodes.

The enhanced stability obtained for the electrodes could be ascribed to the semi-green synthesis approach, which leveraged lemon powder-derived biomolecules and citric acid to minimize agglomeration, enhance the crystallinity (as confirmed by XRD and SEM), reduce defects, and improve the ionic conductivity. In contrast, the chemically synthesized counterparts, such as $Sr_{0.9}Ba_{0.1}CoO_{3-\delta}$, suffer from accelerated capacity fading due to their irregular morphologies and secondary phases (*e.g.*, BaO). Furthermore, the findings also reflect the extraordinary structural integrity of our perovskite framework, even under repeated ion insertion and extraction. The selective substitution of strontium with barium and cerium enhanced the lattice stability and electrochemical reversibility, while the semi-green (LP) and chemical (CA) synthesis methods yielded optimal particle shapes and crystallinity. These factors collectively minimize the degradation mechanisms, such as phase transitions or resistive layer formation, ensuring consistent performance over 5000 cycles, as visually demonstrated in Fig. 9. It is worth noting that 5000 cycles is a widely accepted benchmark in energy-storage research, providing a reliable indicator of material stability for preliminary evaluations. The superior performance of the semi-green-synthesized electrodes, as reflected in both the CV data and the GCD curves, could also be attributed to metallic impurities (*e.g.*, Mg and Ca) from lemon powder, which can boost redox processes, and the larger crystallite sizes, which can reduce the grain boundary resistance, thereby enhancing the electrical conductivity. In addition, the semi-green route followed for the synthesis of perovskite electrodes is more efficient compared to the already existing green routes used to synthesize perovskite electrodes for the supercapacitors. A comparative analysis of some reported green routes is shown in Table 3.

The remarkable stability exhibited by $Sr_{0.9}X_{0.1}CoO_{3-\delta}$ (X = Ce) synthesized through the semi-green route over 5000 cycles, paired with its high capacitance, can position these electrodes and the semi-green routes as promising candidates for next-generation energy-storage devices, where long-term operational reliability and sustainability are paramount.

8. Conclusions

In summary, $Sr_{0.9}X_{0.1}CoO_{3-\delta}$ (X = Ba, Ce) materials were synthesized for the first time as perovskite electrode materials for supercapacitors using an innovative semi-green approach leveraging lemon powder as a bio-chelating agent. This pioneering eco-friendly method achieved high-purity perovskite electrodes with minimal impurities, highlighting its potential for sustainable supercapacitor development. The synthesized electrodes were investigated and compared with chemically synthesized electrodes through XRD, FESEM, EDX, FTIR, and

CV analyses. The XRD analysis validated the successful synthesis of the Ba- and Ce-doped $Sr_{0.9}X_{0.1}CoO_{3-\delta}$ perovskite structure through a semi-green approach with no secondary phase, as evidenced by the characteristic diffraction peaks. The FESEM micrographs revealed a homogenous microstructure with well-defined grains for the semi-green-synthesized $Sr_{0.9}X_{0.1}CoO_{3-\delta}$ (X = Ba, Ce), which was attributed to the synergistic role of biomolecules and bio-chelating agents present in the lemon powder, while the chemically synthesized perovskite anodes exhibited irregular-shaped particles. The EDX mapping confirmed the presence of all the expected elements in all the samples synthesized by both approaches, while FTIR provided insights into the vibrational modes and confirmed the presence of the identical functional groups in all samples, further verifying the structural integrity of the materials synthesized by both approaches. Electrochemical performance evaluations by CV indicated that the semi-green-synthesized $Sr_{0.9}X_{0.1}CoO_{3-\delta}$ (X = Ba, Ce) anodes exhibited promising redox behavior, with distinct oxidation and reduction peaks, compared to the chemically synthesized anodes. It was also observed that Ce-doped $Sr_{0.9}X_{0.1}CoO_{3-\delta}$ exhibited better electrochemical performance than Ba-doped $Sr_{0.9}X_{0.1}CoO_{3-\delta}$, suggesting its good potential for application in energy-storage and -conversion devices. GCD analysis of the $Sr_{0.9}X_{0.1}CoO_{3-\delta}$ (X = Ce) perovskite electrode demonstrated its remarkable electrochemical stability with 88.2% capacity retention after 5000 galvanostatic charge–discharge cycles, demonstrating that strategic A-site substitution could effectively preserve the electrode's performance over extended cycling. In conclusion, it can be deduced that not only did the $Sr_{0.9}X_{0.1}CoO_{3-\delta}$ (X = Ba, Ce) perovskite electrodes demonstrate significant potential as advanced materials for electrochemical storage applications, but the semi-green (LP) route can be effectively used as a synthesis approach for the synthesis of perovskite structures with minimal impurities or ecological impact.

Data availability

The data will be made available upon request.

Conflicts of interest

The authors declare no competing interests or conflicts of interest.

Acknowledgements

The authors extend their appreciation to the Deanship of Research and Graduate Studies at King Khalid University for supporting this work through the Large Research Project under RGP2/125/46.

References

1 S. F. Moosavian, Y. Noorollahi and M. Shoaei, *J. Cleaner Prod.*, 2024, **439**, 140892.
2 A. Al Ojeery, H. ul Hassan, S. A. Al Balawi, M. W. Iqbal, A. M. Afzal and N. M. A. Hadia, *J. Phys. Chem. Solids*, 2023, **180**, 111473.
3 A. Agrawal, A. Gaur and A. Kumar, *J. Energy Storage*, 2023, **66**, 107395.
4 A. Joseph and T. Thomas, *J. Alloys Compd.*, 2024, **971**, 172714.
5 J. F. Pedrayes, M. F. Quintana, G. A. Orcajo, E. E. V. Zaldivar, M. G. Melero and M. F. Cabanas, *Batteries*, 2024, 10.
6 Suyanto, P. A. Darwito, R. A. Wahyuono, M. S. Arifin and B. Sudarmanta, *Int. J. Automot. Technol.*, 2023, **24**, 187–194.
7 M. A. Dar, S. R. Majid, M. Satgunam, C. Siva, S. Ansari, P. Arularasan and S. Rafi Ahamed, *Int. J. Hydrogen Energy*, 2024, **70**, 10–28.
8 F. Wang, X. Wu, X. Yuan, Z. Liu, Y. Zhang, L. Fu, Y. Zhu, Q. Zhou, Y. Wu and W. Huang, *Chem. Soc. Rev.*, 2017, **46**, 6816–6854.
9 Y. Cao, J. Liang, X. Li, L. Yue, Q. Liu, S. Lu, A. M. Asiri, J. Hu, Y. Luo and X. Sun, *Chem. Commun.*, 2021, **57**, 2343–2355.
10 J. Yan, S. Li, B. Lan, Y. Wu and P. S. Lee, *Adv. Funct. Mater.*, 2020, **30**, 1902564.
11 G. Sriram, G. Hegde, K. Dhanabalan, Y. Kalegowda, D. Mouraliraman, R. S. Vishwanath, M. Kurkuri and T. H. Oh, *J. Energy Storage*, 2024, **94**, 112454.
12 *3D Printed Conducting Polymers: Fundamentals, Advances, and Challenges*, ed. R. K. Gupta, CRC Press, 1st edn, 2024, DOI: 10.1201/9781003415985.
13 Q. Zhang and B. Wei, *Small*, 2024, 2311957.
14 C. Costentin, T. R. Porter and J. M. Savéant, *ACS Appl. Mater. Interfaces*, 2017, **9**, 8649–8658.
15 F. Escobar-Teran, H. Perrot and O. Sel, *Physchem*, 2023, **3**, 355–384.
16 *Pseudocapacitors: Fundamentals to High Performance Energy Storage Devices*, ed. R. K. Gupta, Springer Nature, Switzerland, Germany, 2023.
17 H. Hosseini and S. Shahrokhian, *Chem. Eng. J.*, 2018, **341**, 10–26.
18 C.-C. Hu, W.-C. Chen and K.-H. Chang, *J. Electrochem. Soc.*, 2004, **151**, A281.
19 M. Song, J. Zhao, H. Li, X. Yu, X. Yang, L. Zhang, Z. Yin and X. Wang, *J. Electroanal. Chem.*, 2020, **857**, 113755.
20 X. Xu, W. Wang, W. Zhou and Z. Shao, *Small Methods*, 2018, **2**, 1–35.
21 K. Brezesinski, J. Wang, J. Haetge, C. Reitz, S. O. Steinmueller, S. H. Tolbert, B. M. Smarsly, B. Dunn and T. Brezesinski, *J. Am. Chem. Soc.*, 2010, **132**, 6982–6990.
22 G. F. Liu, P. P. Ma, Y. Qiao, R. H. Xu, D. M. Huang, R. Y. Hu, L. Y. Liu, G. H. Jiang and M. Demir, *J. Energy Storage*, 2022, **52**, 104942.
23 W. W. Zhang, Y. Wang, Y. C. Li and X. Y. Zhang, *J. Ind. Eng. Chem.*, 2024, **139**, 199–212.
24 C. Yang, Y. Gan, M. Lee, C. Ren, K. S. Brinkman, R. D. Green and X. Xue, *J. Mater. Chem. A*, 2020, **8**, 10450–10461.
25 X. Lv, H. Chen, W. Zhou, S.-D. Li and Z. Shao, *J. Mater. Chem. A*, 2020, **8**, 11292–11301.

26 H. Zhou, G. Qi, W. Li, W. Song and Z. Yuan, *Langmuir*, 2024, **40**(27), 14027–14036.
27 S. Hu, S. Gu, C. Yang, J. Cheng, J. Xu, J. Pu and B. Chi, *J. Power Sources*, 2024, **602**, 234389.
28 S. Li, Y. Liu, C. Cai, K. Xue, L. Bian and S. An, *J. Power Sources*, 2024, **592**, 233932.
29 F. Xiao, X. Zhang, F. Hu and J. Zhang, *Mater. Chem. Phys.*, 2005, **94**, 221–225.
30 M. A. Salguero Salas, J. M. De Paoli, O. E. Linarez Pérez, N. Bajales and V. C. Fuertes, *Microporous Mesoporous Mater.*, 2020, **293**, 109797.
31 H. Li, J. Yu, Y. Gong, N. Lin, Q. Yang, X. Zhang and Y. Wang, *Sep. Purif. Technol.*, 2023, **307**, 122716.
32 D. Gupta, A. Boora, A. Thakur and T. K. Gupta, *Environ. Res.*, 2023, **231**, 116316.
33 K. Y. Park, Y. Seo, K. B. Kim, S. J. Song, B. Park and J. Y. Park, *Enhanced proton conductivity of yttrium-doped barium zirconate with sinterability in protonic ceramic fuel cells*, Elsevier B.V., 2015, vol. 639.
34 M. Irshad, M. Khalid, M. Rafique, N. Ahmad, K. Siraj, R. Raza, M. Sadiq, M. Ahsan, A. Ghaffar and A. Ashfaq, *RSC Adv.*, 2021, **11**, 14475–14483.
35 D. Yun, J. Kim, S.-J. Kim, J.-H. Lee, J.-N. Kim, H. Yoon, J. Yu, M. Kwak, H. Yoon, Y. Cho and C.-Y. Yoo, *Energies*, 2018, **11**, 3083.
36 K.-Y. Park, Y. Seo, K. B. Kim, S.-J. Song, B. Park and J.-Y. Park, *J. Alloys Compd.*, 2015, **639**, 435–444.
37 N. Singh, M. Seshadri, M. S. Pathak and V. Singh, *Solid State Sci.*, 2019, **87**, 163–170.
38 M. D. Gonçalves, P. S. Maram, A. Navrotsky and R. Muccillo, *Ceram. Int.*, 2016, **42**, 13689–13696.
39 A. Majedi, A. Abbasi and F. Davar, *J. Sol-Gel Sci. Technol.*, 2016, **77**, 542–552.
40 J. Luo, J. Zhang, A. Wang, Y. Liu, J. Cheng, Y. Zhao, D. Yan, L. Jia and J. Li, *Int. J. Hydrogen Energy*, 2024, **56**, 871–879.
41 A. S. Salwa, A. E.-S. Ahmed, H. S. Wasly and M. S. Abd El-Sadek, *ECS J. Solid State Sci. Technol.*, 2022, **11**, 103005.
42 A. Modwi, K. K. Taha, L. Khezami, A. S. Al-Ayed, O. K. Al-Duaij, M. Khairy and M. Bououdina, *J. Inorg. Organomet. Polym. Mater.*, 2020, **30**, 2633–2644.
43 W. Zhu, W. Deng, Z. Li, Z.-Y. Shen, X. Shi, F. Song, W. Luo, Z. Wang and Y. Li, *J. Mater. Sci.: Mater. Electron.*, 2022, **33**, 26861–26869.
44 D. A. Agarkov, M. A. Borik, G. M. Korableva, A. V. Kulebyakin, B. E. Komarov, I. E. Kuritsyna, E. E. Lomonova, F. O. Milovich, V. A. Myzina, V. A. Pankratov, N. Y. Tabachkova and D. M. Zakharov, *J. Solid State Electrochem.*, 2024, **28**, 1901–1908.
45 G. Kimmel, A. Sahartov, Y. Sadia, Z. Porat, J. Zabicky and E. Dvir, *J. Mater. Res. Technol.*, 2021, **12**, 87–99.
46 K. C. Suresh, S. Surendhiran, P. Manoj Kumar, E. Ranjth Kumar, Y. A. S. Khadar and A. Balamurugan, *SN Appl. Sci.*, 2020, **2**, 1735.
47 R. Varghese, C. O. Sreekala, S. Kurian and J. K. Thomas, *J. Mater. Sci. Mater. Electron.*, 2023, **34**, 1–16.
48 M. Mahiuddin and B. Ochiai, *RSC Adv.*, 2021, **11**, 26683–26686.
49 R. Javed, M. Usman, S. Tabassum and M. Zia, *Appl. Surf. Sci.*, 2016, **386**, 319–326.
50 C. V. Restrepo and C. C. Villa, *Environ. Nanotechnol., Monit. Manage.*, 2021, **15**, 100428.
51 M. Baladi, M. Amiri, P. Mohammadi, K. Salih Mahdi, Z. Golshani, R. Razavi and M. Salavati-Niasari, *Arabian J. Chem.*, 2023, **16**, 104646.
52 P. K. Upadhyay, V. K. Jain, S. Sharma, A. K. Shrivastav and R. Sharma, Green and chemically synthesized ZnO nanoparticles: A comparative study, in *IOP Conference Series: Materials Science and Engineering*, IOP Publishing, 2020, vol. 798, no. 1, p. 012025, DOI: 10.1088/1757-899X/798/1/012025.
53 M. Irshad, N. Kousar, M. B. Hanif, A. N. Tabish, A. Ghaffar, M. Rafique, K. Siraj, Z. Aslam, M. A. Assiri, M. Imran, M. Mosiałek, Z. Zmrhalova and M. Motola, *Sustainable Energy Fuels*, 2022, **6**, 5384–5391.
54 L. Zhang, Y. Yin, Y. Xu, S. Yu and L. Bi, *Sci. China Mater.*, 2022, **65**, 1485–1494.
55 D. Kubba, I. Ahmed, A. Roy, P. Kour, C. S. Yadav, S. K. Sharma, K. Yadav and K. K. Haldar, *ACS Appl. Nano Mater.*, 2024, **7**, 1536–1547.
56 K. Zulfa, B. Zahara, A. A. Afkauni, P. Y. Diah Maulida, S. Hartati, I. Mulyani, A. Yudhowijoyo, L. J. Diguna, M. H. Mahyuddin, D. Onggo, M. D. Birowosuto and Arramel, *Mater. Today Proc.*, 2024, DOI: 10.1016/j.matpr.2024.03.058.
57 M. He, M. Alomar, A. S. Alqarni, N. Arshad, M. Akbar, M. Yousaf, M. S. Irshad, Y. Lu and Q. Liu, *Nanomaterials*, 2023, **13**(8), 1420.
58 X. Luan, X. Wang, T. Zhang, L. Gan, J. Liu, Y. Zhai, W. Liu, L. Wang and Z. Wang, *Compounds*, 2024, **4**, 268–287.
59 R. W. Utami, R. A. Rafsanjani and D. Triyono, *J. Phys.:Conf. Ser.*, 2019, **1153**, 0–5.
60 A. J. McQuillan, M. Osawa, D. Peak, B. Ren and Z. Q. Tian, *Pure Appl. Chem.*, 2019, **91**, 2043–2061.
61 S. M. Bashir and H. Idriss, *J. Chem. Phys.*, 2020, **152**, 044712.
62 M. A. Ahmed, M. S. Selim and M. M. Arman, *Mater. Chem. Phys.*, 2011, **129**, 705–712.
63 M. Sheoran, R. Sharma, S. Chaudhary, A. Dawar, S. Ojha, A. Verma, A. Srivastava and O. P. Sinha, *Appl. Phys. A: Mater. Sci. Process.*, 2023, **129**, 549.
64 L. E. Garcia and M. A. Sozen, *J. Mater. Chem. A*, 2015, 1–12.
65 Y. Belazougui, A. Dib, T. Hadjersi, R. Maizia, A. Thomas and S. Martemianov, *ChemistrySelect*, 2024, **9**, e202400750.
66 J. P. Cheng, S. Q. Gao, P. P. Zhang, B. Q. Wang, X. C. Wang and F. Liu, *J. Alloys Compd.*, 2020, **825**, 153984.
67 S. Guo, W. Chen, M. Li, J. Wang, F. Liu and J. P. Cheng, *Electrochim. Acta*, 2018, **271**, 498–506.
68 T. Zhu, S. J. Zheng, Y. G. Chen, J. Luo, H. B. Guo and Y. E. Chen, *J. Mater. Sci.*, 2014, **49**, 6118–6126.
69 C. Li, H. Chen, R. Nie, Y. Yang and H. Zhou, *J. Mater. Sci.: Mater. Electron.*, 2023, **34**, 1–14.
70 E. Bilgin Simsek and Ö. Tuna, *J. Phys. Chem. Solids*, 2023, **176**, 111276.
71 E. Smith, S. Škapin and R. Ubic, *J. Alloys Compd.*, 2020, **836**, 155475.

72 N. Lei, Y. Qiao, G. Liu, R. Xu, G. Jiang, M. Demir and P. Ma, *Mater. Chem. Phys.*, 2022, **288**, 126389.
73 Y. Qiao, G. Liu, R. Xu, R. Hu, L. Liu, G. Jiang, M. Demir and P. Ma, *Electrochim. Acta*, 2023, **437**, 141527.
74 J. He, Y. Zhou, S. Wu, L. Jin, J. Cao, M. Demir and P. Ma, *Inorg. Chem.*, 2024, **63**, 13755–13765.
75 Y. Wu, X. Jia, H. Zhang, F. Zhou, Z. Fu, X. Jia, Z. Li, F. Liu, L. Wang and Z. Xiao, *J. Energy Storage*, 2023, **62**, 106855.
76 O. Karaman, İ. A. Kariper, S. Korkmaz, H. Karimi-Maleh, M. Usta and C. Karaman, *Fuel*, 2022, **328**, 125298.
77 M. Abdullah, P. John, K. F. Fawy, S. Manzoor, K. Y. Butt, A. G. Abid, M. Messali, M. Najam-Ul-Haq and M. N. Ashiq, *RSC Adv.*, 2023, **13**, 12009–12022.
78 T. N. V. Raj, P. A. Hoskeri, H. B. Muralidhara, C. R. Manjunatha, K. Y. Kumar and M. S. Raghu, *J. Electroanal. Chem.*, 2020, **858**, 113830.
79 Z. U. Rehman, M. A. Raza, A. Tariq, U. N. Chishti, M. F. Maqsood, N. Lee, M. H. Awais, S. M. Z. Mehdi and A. Inam, *J. Energy Storage*, 2020, **32**, 101951.
80 P. M. Shafi, N. Joseph, A. Thirumurugan and A. C. Bose, *Chem. Eng. J.*, 2018, **338**, 147–156.
81 S. Nayak, A. A. Kittur and S. Nayak, *Curr. Res. Green Sustainable Chem.*, 2022, **5**, 100292.
82 M. Riaz, S. M. Ali, S. D. Ali, M. Sadiq and M. A. Shakoori, *Diamond Relat. Mater.*, 2024, **144**, 110938.
83 R. Kumar, S. Gokul, F. Ran, S. Sambasivam, K. A. Alrashidi and R. Thangappan, *J. Energy Storage*, 2024, **98**, 113231.